RSC Advances

PAPER

View Article Online
View Journal | View Issue

Cite this: *RSC Adv.*, 2025, **15**, 8553

Exploring the sensing properties of pH-sensitive carbazole-based AIE emitters and their applications in paper strip sensing†

Diksha Saluja, Prakash Seenu, Saravanan Enbanathan and Sathiyanarayanan Kulathu Iyer *

Received 19th December 2024
Accepted 11th March 2025

DOI: 10.1039/d4ra08882d

rsc.li/rsc-advances

A novel carbazole-coupled phenanthridine molecule with an intense blue emissive fluorescence was produced through a two-step synthesis of 5-(4-(9*H*-carbazol-9-yl)phenyl)-7,8,13,14-tetrahydrodibenzo[*a*,*i*]phenanthridine (**DSPH**). This blue probe shows a good thermal and electrochemical stability. It has been used for sensing trifluoracetic acid (TFA) with a limit of detection (LoD) value of 198 pM. The probe tends to show aggregation induced emission (AIE) characteristics. Additionally, the experimental data were supported by DFT analysis.

1. Introduction

The demand for organic materials in optoelectronics has been steadily increasing in the 21st century. These materials, such as poly(phenylenevinylene) (PPV) and poly(3-hexylthiophene) (P3HT), have applications in solar cells and OLED devices. In addition to these polymers, scientists have been using small molecules like organic fluorophores, such as fluorescent dyes. Another emerging field is the use of perovskites, a hybrid generation of organic and inorganic materials. All these materials are currently being utilized for various optoelectronic applications based on their specific properties. The fluorescent dyes are also promising materials for use in these applications.[1] These luminophores are preferred by scientists over expensive phosphorescent materials. There are several examples of organic moieties that are specifically employed in the synthesis of fluorescent dyes like triphenylamine, pyrene, and carbazoles.[2] The choice of the appropriate organic moiety depends on various factors like hole transporting and electron transporting ability, thermal stability, and resistance to thermal and electrochemical degradation. Another striking feature to be considered is the band gap and emission properties of the fluorophore moiety.[3] Since the discovery of the Aggregation Induced Emission (AIE) property in some organic moieties by Tang *et al.* in 2001,[4] there has been consistent development in the field to design efficient organic moieties incorporated with the AIE property to enhance their emission properties and make effective materials for use in optoelectronics. Unlike the usual effect observed in organic fluorophores, where the emission intensity is quenched in the solid state or when an aggregate is formed, known as Aggregate-Caused Quenching (ACQ), AIE tends to enhance the emission intensity of a particular probe and overcome the phenomenon of ACQ. The mechanism that follows the overcoming of the ACQ effect is Restricted Intramolecular Rotation (RIR), which, on the formation of an aggregate, restricts the rotation of the probe in solution and hence reduces the non-radiative decay pathways for the concerned probe, resulting in enhanced fluorescence emission.[5] This change in the photophysical property of a probe makes them ideal substrates to be employed as materials for OLEDs, organic lasers, organic solar cells, bioimaging, and chemical sensors. A significant number of molecules have been designed that work as AIE emitters and are then employed in the applications. Along with this, these fluorescent organic materials are also used as optical sensors for various analytes due to the presence of a heterocyclic entity.[6–8] Some renowned examples of AIE emitter hosts include tetraphenyl ethylene derivatives, carbazole-based materials, and triphenylamine derivatives, as shown in Fig. 1. Structures (**i–iii**) represent tetraphenyl ethylene derivatives as AIE hosts for optoelectronic applications, structures (**iv** and **v**) are triphenylamine moieties decorated with carbazole substituents, and structures (**vi** and **vii**) are carbazole-based AIE emitters for OLED applications.[5,9–13] According to the literature, there have been a lot of reports on hosts like tetraphenyl ethylene derivatives, triphenylamine, and phenanthroimidazole but carbazoles as the core organic moiety for designing AIE active material is not that much exploited. Carbazole is a planar moiety having a rigid structure. It possesses a blue light emitting fluorescence and has good electron transporting abilities, making it one of the ideal substrate choices for designing such materials. Along with that carbazole can be easily functionalized further helping in enhancing the AIE property.[14] There have been a certain

Department of Chemistry, School of Advanced Sciences, Vellore Institute of Technology, Vellore, 632014, India. E-mail: sathiya_kuna@hotmail.com

† Electronic supplementary information (ESI) available. See DOI: https://doi.org/10.1039/d4ra08882d

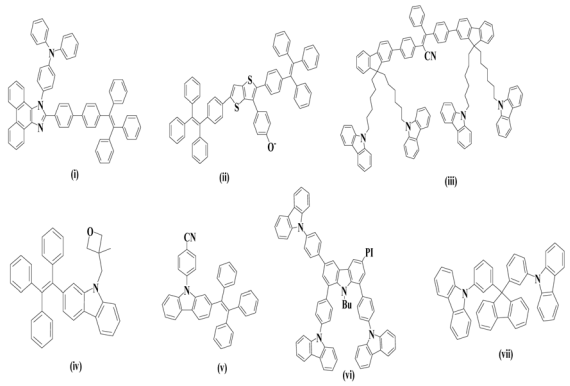

Fig. 1 AIE emitter hosts described in the literature for OLED applications.

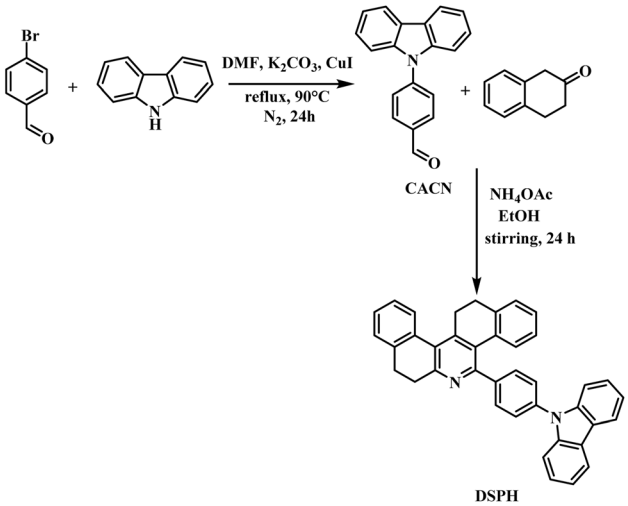

Scheme 1 Synthesis of carbazole-coupled phenanthridine.

number of reports using carbazole as an AIE emitter and employed as a material for optoelectronics. A. Sharma *et al.*, (2021) designed a probe featuring substituted carbazole including a phenanthroimidazole unit in a two-step reaction. This probe exhibited AIE properties and was further characterized *via* various other photophysical, thermal, and electrochemical properties. The material was also subjected to check for any possible sensing, the compound was showing a response for trifluoracetic acid, TFA resulting in a new moiety formation from the protonation of the phenanthroimidazole unit. Also, the material was investigated for theoretical investigations *via* DFT studies for the optimization of geometry and calculation of HOMO and LUMO values along with the energy band gap. This material can be further employed in forming a blue OLED device.[15] C.-Y. Ho *et al.* developed a carbazole-based material through a two-step synthetic process. The first step involved a Suzuki coupling reaction between carbazole, boronic acid pinacol ester, and bromo triphenylethylene. In the second step, the resulting compound was reacted with bromobenzonitrile using a Buchwald–Hartwig reaction. This formed probe was utilized in the formation of white OLEDs (WOLEDs) and showed significant AIE property and a high potential to be used for other electronic applications.[9] In 2022, Seenan, S. *et al.*, created a phenanthridine derivative in a reaction with 2-tetralone which was further used for sensing applications. A similar approach was used as the basis of this work.[16] This work delved into forming a carbazole-coupled phenanthridine probe which could be employed as a material for dual applications for optoelectronics and sensing. It involves a two-step reaction. The first step leads to the formation of carbazole coupled with benzaldehyde (**CaCN**) (see Scheme 1). **CaCN** is a reported compound,[17,18] and it was synthesized *via* the Ullman Coupling reaction, with some deviations from the literature. Jie Zhang *et al.* used iodobenzaldehyde and crown ether for dissolving metal salts.[19] In contrast, our method excluded the use of crown ether and achieved the synthesis in fewer reaction hours. **CaCN** was further coupled with 2-tetralone and ammonium acetate as per the standard procedure from our group[20] to enhance its fluorescent sensory properties. Further, the carbazole-coupled phenanthridine probe was subjected to standard analytical methods, first for the structural confirmation *via* (^{1}H, ^{13}C) NMR spectroscopy, FT-IR & HRMS. Later, its photophysical properties were studied such as Aggregation Induced Emission (AIE), solvatochromism in solvents of different polarity and Brønsted acid sensing. Also, the material was subjected to thermal and electrochemical studies *via* thermogravimetric analysis (TGA) and cyclic voltammetry (CV). To aid the experimental process, it was further supported by theoretical investigations to optimize the structure and calculation of energy band gap values.

2. Materials

All the compounds were purchased from commercial providers (Sigma Aldrich and TCI chemicals), and they were utilized without purification. NMR spectroscopic examination of ^{1}H and ^{13}C was conducted using Bruker 400 MHz and 100 MHz instruments, with spectral data values reported in parts per million (ppm, δ). The UV-vis absorption and emission spectra were recorded using Hitachi-2910 and Hitachi F-7000 spectrophotometers, respectively. A JASCO FT-IR 4600 and a Joel GC Mate II GC-Mass Spectrometer were used to obtain infrared spectrum (IR) and high-resolution mass spectrum (HRMS), respectively. Thermogravimetric analysis was performed on SDT Q600 and cyclic voltammetry study was carried out on C–H instrument electrochemical workstation.

2.1 Stock solution preparation

The stock solution of **DSPH** (1×10^{-3}) was prepared by dissolving in THF solution. The TFA analyte was prepared in a double distilled water medium (1×10^{-3}). The absorption and emission spectra were recorded in THF.

3. Results and discussion

3.1 Synthesis and characterization

3.1.1 Synthesis of 4-(9*H*-carbazol-9-yl)benzaldehyde. In a 100 mL round-bottomed flask, 1 g, (1 mmol) of 9*H*-carbazole

was taken and to it, K_2CO_3 (1.6 g, 2 mmol), copper iodide (0.2 g, 0.2 mmol) and later 4-bromobenzaldehyde (1.1 g, 1 mmol) were added in presence of 10 mL of DMF as solvent. The flask was kept for reflux in nitrogen atmosphere at 90 °C for 24 hours. The reaction was monitored using TLC and after completion of the reaction the solution was added to crushed ice and kept for stirring, a yellowish-brown product was obtained and it was filtered which was further purified by column chromatography to obtain a white solid (0.85 g, 59%), in a hexane:ethyl acetate mixture and the melting point was 134–136 °C. ^{1}H-NMR (400 MHz, $CDCl_3$, δ, ppm): 10.1 (s, 1H,-CHO), 8.27–8.18 (m, J = 7.68 Hz, 4H, Ph-H), 7.90 (d, J = 8.32 Hz, 2H, Ph-H), 7.53 (d, J = 8.2 Hz, 2H, Ph-H), 7.44–7.47 (t, J = 7.92; 7.28 Hz, 2H, Ph-H), 7.31–7.35 (t, J = 7.68; 7.04 Hz, 2H, Ph-H). $\{^1H\}^{13}$C-NMR (100 MHz, $CDCl_3$, δ, ppm): 192.67, 142.66, 139.91, 135.03, 131.87, 127.15, 126.9, 123.7, 121.25, 121.12, 110.3.

3.1.2 Synthesis of 5-(4-(9*H*-carbazol-9-yl)phenyl)7,8,13,14-tetrahydrodibenzo[*a*,*i*]phenanthridine (DSPH). The aldehyde obtained in the first step was taken into a 100 mL round-bottomed flask (1 g, 1 mmol). To it, 15 mL of ethanol was added and warmed. Followed by it, ammonium acetate (0.45 g, 1.5 mmol) was added and the lid was closed and stirred for ten minutes. Later, 2-tetralone (1 mL, 2 mmol) was added to the flask and the setup was kept for stirring for 24 hours. The reaction was monitored by TLC with a R_f = 0.6 and a brown product was filtered and purified by column chromatography in a 3% hexane: ethyl acetate mixture, yielding a light brown solid (0.4 g, 21%), melting point was 301–303 °C. ^{1}H-NMR (400 MHz, $CDCl_3$, δ, ppm): 8.07 (d, J = 7.8 Hz, 2H, Ph-H), 8.05 (d, J = 7.8 Hz, 2H, Ph-H), 7.63–7.61 (d, J = 8.2 Hz, 3H, Ph-H) 7.35–7.39 (m, 4H, Ph-H), 7.27–7.30 (m, 1H, Ph-H), 7.19–7.25 (m, 5H, Ph-H), 7.10–7.14 (m, 1H, Ph-H), 6.92–6.97 (m, 2H, Ph-H), 3.05–3.12 (m, 4H, Cy-H), 2.90–2.93 (t, J = 7.48; 5.84 Hz, 2H, Cy-H), 2.72–2.75 (t, J = 6.8; 6.2 Hz, 2H, Cy-H) [*Ph – phenyl ring, *Cy – cyclohexane ring]. $\{^1H\}^{13}$C-NMR (100 MHz, $CDCl_3$, δ, ppm): 158.35, 152.93, 145.96, 141.14, 140.80, 139.71, 138.91, 137.23, 132.95, 132.89, 137.47, 129.69, 129.16, 128.77, 127.96, 127.88, 127.84, 127.33, 127.13, 126.91, 126.14, 125.99, 125.71, 123.45, 120.32, 119.97, 109.87, 33.26, 29.58, 29.49, 29.25. Then we recorded FT-IR: 2943 (C–H), 1600 (C=C aromatic), 1450.06 (C–H bend), 1105 (C–H aliphatic stretch), 1511.4 (C=N stretch), 1223.7 (C–N stretch). Then we confirmed by HRMS analysis, calculated mass = 524.2252m/z, and observed mass with proton adduct (M + H): 525.2331m/z.

3.2 Solvatochromism

To study the effect of solvent polarity on the probe's photophysical properties, it was tested for changes in absorption and emission in solvents of varying polarity from chloroform to DMSO. The results of the absorption and emission spectra are shown in Fig. 2a and b and the photophysical parameters are given in ESI Table 1.† The absorption and emission plots were normalized to assess the change concerning different solvents, it was predicted that the absorption spectrum consisted of two main shoulder peaks representing π–π* & n–π* transition. The plot in Fig. 2a indicates that there remains no specific change

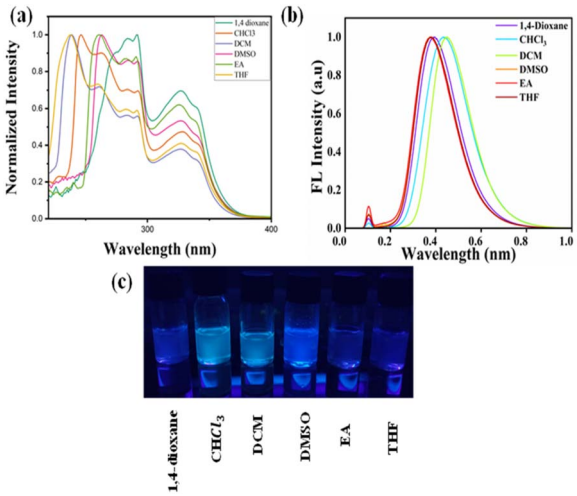

Fig. 2 Solvatochromism effect on DSPH in the presence of solvents of various polarities. (a) Absorption spectrum, (b) emission spectrum, (c) bottle images of probe.

compared to other solvents. Based on polarity, the spectrum (λ_{max}) in least polar solvents chloroform and DCM move a little towards the increasing wavelength region. Further in the series ethyl acetate follows the trend with a more shift than the former two. DMSO and 1,4-dioxane gave a significant shift towards higher wavelength values. These results shape the fact that the probe shows a positive solvatochromism effect or bathochromic shift with increasing solvent polarity. It further specifies that the probe is more polar in excited states and hence it gets stabilized by diminishing the energy gap between the ground and excited state in the vicinity of polar solvents. The emission spectrum also has rated some changes concerning the change in solvent polarity. Fig. 2b precisely reflects the change in emission wavelength in the case of DMSO, DCM and chloroform. Further, the photophysical parameters related to the study were tabulated and photophysical properties such as absorption and emission maxima values, full-width half maxima (FWHM) and Stokes shift values were calculated and mentioned in ESI Table 1.† The calculations reveal that Stokes shift value was highest in the case of DMSO, followed by DCM and chloroform which depicts that there was a higher energy loss due to factors like solvent–solvent interaction and solvent polarity.

3.3 Aggregation induced emission

There has been a rapid increase in emission that shows aggregation-induced emission due to the formation of aggregates. The probe **DSPH** was completely soluble in THF and insoluble in water. This property was utilized for the method of aggregate formation, wherein a maximum emission was observed at a water percentage of 50% and accordingly, the THF-to-water ratio was maintained in the solution.

This ratio facilitated the formation of aggregates. The aggregates were then prepared using the drop casting method, where the THF–water mixture was carefully dropped onto glass strip sheets and allowed to dry. The resulting aggregates were

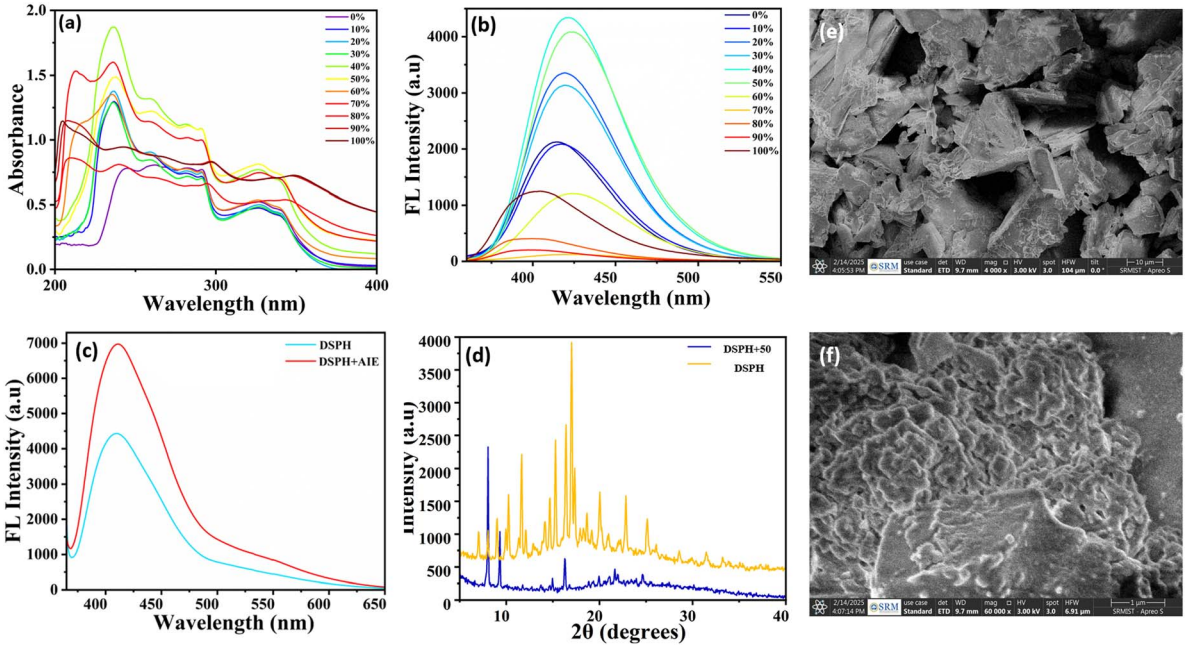

Fig. 3 Aggregation studies of **DSPH** in THF:water mixtures. (a) Absorption spectrum, (b) emission spectrum, (c) solid state emission of probe and aggregate, (d) XRD of probe **DSPH** and aggregate at $f_w = 50\%$, (e) SEM image of powder **DSPH**, (f) SEM image of aggregate (**DSPH** + 50).

further studied using powder X-ray diffraction (p-XRD) to analyze their crystalline structure, dynamic light scattering (DLS) to study emission at solid stage and scanning electron microscopy (SEM) to examine their surface morphology. It showed a blue fluorescence in the solvent, THF. The compound's emission spectrum was observed in Fig. 3b by varying percentages of THF–H_2O fractions. Upon the addition of water fractions, the compound showed an increase in fluorescence emission intensity. The maximum emission intensity was observed at 422 nm attributing to 50% of the THF–H_2O mixture. The compound showed an increase in emission intensity up to 50% of THF–H_2O and a decrease in emission intensity was observed from 60–100% which could be attributed to aggregation-caused quenching (ACQ) in higher water fractions. This phenomenon of aggregation-induced enhanced emission (AIE) is attributed to the restricted intramolecular rotation in the probe upon the addition of water fractions causing it to show a higher emissive fluorescence. The reason for ACQ in case of higher water fractions might be attributed to collisional quenching, as a result having diminished emission intensity. Also, the formation of dimers in excited state (excimers) or complex between ground and excited state (exciplex) can also lead to ACQ in higher water concentrations.[21] The solid-state emission of the probe and its aggregates was studied to better understand Aggregation-Induced Emission (AIE). It was found that the emission intensity increased significantly in the solid state with aggregate formation compared to the probe alone (Fig. 3c). This confirms that the probe exhibits AIE, both in solution during aggregate formation and in the solid state.[22–24] The enhanced emission results were supported by DLS experiments as well which revealed a mean aggregate diameter of 87.5 nm, indicating significant aggregation in the sample (ESI Fig. S9†). Furthermore, the sample was polydisperse, showcasing a diverse population of aggregates. These findings align with the AIE phenomenon, where the enhanced emission is attributed to the formation of varied-sized aggregates in the solid state and in solution.[25,26] Additionally, the morphology of the aggregates was also studied by p-XRD and SEM analysis. The XRD revealed that, at $f_w = 50\%$ there is a change in the peaks pattern and the sample changes from crystalline to somewhat amorphous at its aggregated state (Fig. 3d). The same was verified from SEM images which showed a clear image of sharp spear-like pattern in case of probe **DSPH** (Fig. 3e) and in case of aggregate it shows a lump formation (Fig. 3f) in the image unlike the typical sharp spears like structure, which indicates positive aggregate formation.

3.4 Thermal properties

For checking the thermal stability of the probe **DSPH**, it was tested by thermogravimetric analysis (TGA) which was performed under an inert atmosphere with nitrogen at a heating rate of 20 °C min^{-1} (ESI Fig. S7†). The initial 10% decomposition was attributed to moisture content and gases. The probe posed higher thermal stability as the onset temperature was observed to be at 370 °C. Almost 70% of the compound was decomposed. At 470 °C no further decomposition was observed and 24% of the probe was left as residue. The high value of T_{onset} may have an effective long stability in OLEDs and other optoelectronic devices. The current work was compared with other carbazole-based probes for the onset decomposition temperature values (ESI Table S2†), and was found that the current probe lies in similar temperature ranges as other carbazole-based probes. This was further confirmed by comparing the stability of probe **DSPH** with the recently developed probes.

3.5 Electrochemical properties

The electrochemical property of the probe was examined by obtaining cyclic voltammograms CV to introspect about the electrochemical properties.[27] Tetrabutylammonium perchlorate (TBAP) was used as the supporting electrolyte (0.1 M) and ferrocene was employed as the internal standard. A three-electrode system was used wherein silver was the reference electrode, platinum was the working electrode, and platinum wire was the counter electrode. The corresponding cyclic voltammogram was recorded at a scan rate of 50 mV s^{-1} under nitrogen atmosphere and is displayed in ESI Fig. S8.† The plot indicated that the irreversibility of the reaction with just an oxidation potential peak, which is attributed to the loss of electrons from carbazole present in the probe. Additionally, the HOMO and LUMO values were calculated from the CV.[28,29] The onset oxidation potential (E_{ox}) of **DSPH** was determined to be 0.92 V. Based on the equation, [HOMO = $-(4.40 + E_{ox})$], the energy level of HOMO of **DSPH** was calculated to be −5.32 eV. Further, the LUMO energy level was calculated using the equation, [LUMO = $-$(HOMO + ΔE_g)], which comes out to be −1.56 eV. The optical bandgap of the compound was determined by Tauc plot method given by the formula 1240/λ where λ is the wavelength of absorbed light in nanometres and calculated to be 3.75 eV. The value is consistent with the band gap determined from DFT calculations, 3.79 eV. The values for HOMO and LUMO are mentioned in ESI Table S3.†

3.6 Selectivity studies

The need to develop a fluorescent sensor for TFA is necessary, since there is a lot of consumption of this volatile and toxic acid in the field of organic chemistry specifically synthesis.[30] The presence of TFA vapours in environment is harmful for health and it is a significant factor in ozone layer depletion as well. Compared to other methods for its detection fluorescent sensors hold more potential due to relative ease of simplicity and high sensitivity and selectivity towards analyte.[31] To understand the behaviour of the probe as a possible sensor, selectivity studies were performed and the absorption as well as emission spectrum of the probe with certain acid analytes was recorded to understand the possible interacting analyte. The choice of acid analytes included [phosphoric acid (PPA), propionic acid (PPA-2), sulphuric acid (H_2SO_4), methane sulfonic acid (MSA), methacrylic acid (MAA), heptanoic acid (HTA), oleic acid (OA), acetic acid (AcOH), HNO_3, HCl and TFA]. The absorption spectrum in Fig. 4a reveals the major transitions in the case of the probe at 294 nm and 336 nm are π–π* and n–π* respectively. While most other analytes did not show any disturbance in the absorption spectrum, there was a significant change in the plot in the case of TFA which shows that the probe binds preferentially with TFA. Furthermore, the emission spectrum Fig. 4b revealed that in the case of other acid analytes, there is no significant change in the fluorescence intensity of the probe whereas, when the probe interacts with TFA, the emission spectrum recognizes a quenching of fluorescence intensity, thereby indicating that the probe shows high selectivity towards TFA.[32] The interference studies were done for the

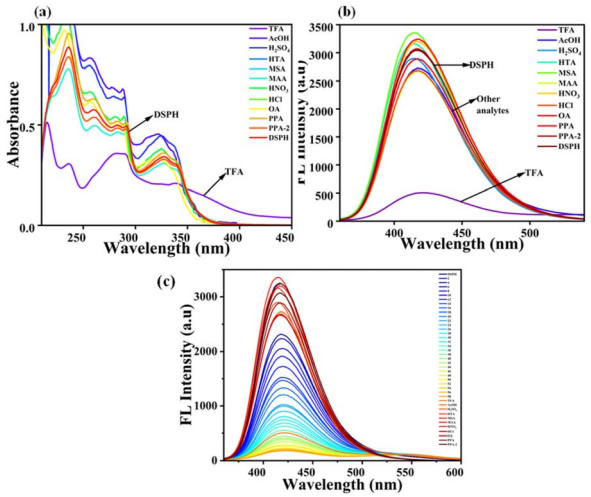

Fig. 4 Selective acid sensing by the probe, (a) absorption, and (b) emission spectrum revealing quenching by TFA compared to other acid analytes, (c) competitive titrations to study interference from other acid analytes.

probe **DSPH** in presence of other acid analytes and it showed that the probe selectively formed a complex with TFA in presence of other acid analytes as well Fig. 4c. In the same medium, TFA equivalents were increased to observe similar quenching mechanism for **DSPH + TFA** complex as it was observed when the study was done without other interfering analytes. Moreover, it was concluded that there was no interference effect of other acid analytes on formation of complex between **DSPH** and TFA.

3.7 Acid induced spectroscopic variations

To investigate the fluorescent sensing property of the probe, it was made to observe the effect of an acid analyte (TFA) to determine the change in its photophysical properties using THF as a solvent. The choice of TFA was made as a analyte of the probe based on the selectivity studies in the previous section. The changes in absorption and emission spectrum due to the complex formation of the probe with TFA are observed in Fig. 5a and b. The probe is sensitive to TFA owing to the protonation of the phenanthridine unit in it. The probe absorption spectra

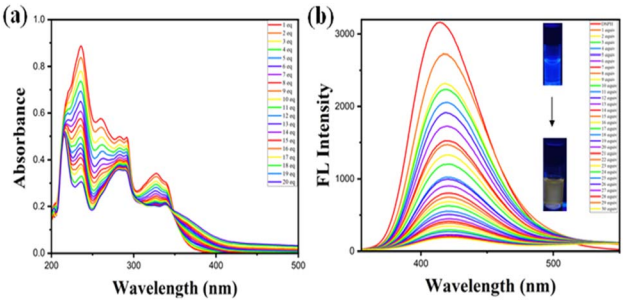

Fig. 5 Acid-induced spectroscopic variations. (a) Absorption spectrum, (b) emission spectrum of probe DSPH with TFA analyte.

showed several shoulder peaks, of which peak at 236 nm corresponds to π–π* and another absorption band owing to n–π* transition at 328 nm. With the increase in TFA concentration, the probe reached an isosbestic point at 348 nm. The probe when subjected to emission studies revealed that upon increase in TFA concentration led to quenching of the probe emission intensity from 0 to 3 equivalents of TFA. This plot reveals that the probe is sensitive towards acid owing to the protonation of phenanthridine moiety and gets quenched upon the addition of increasing equivalents of TFA. The studies were repeated 3–4 times and reproduced similar results. The emission studies with increasing equivalents of TFA revealed a linear correlation between the relative intensity (I/I_0 at 430 nm) and the TFA concentration. This relationship was established using both the derived calibration plot and the Benesi–Hildebrand plot and the stoichiometry was defined using Jobs plot as 1 : 1 (ESI Fig. S10†). The observed linearity suggests a predictable change in fluorescence intensity with incremental additions of TFA, thus providing a dependable method for quantifying TFA concentrations. The linear equation derived from the plot was $y = 8.68626x + 1.11253$, where x is the concentration of TFA and y is the absorption intensity at 430 nm. The association constant was determined to be 1.28×10^6 M^{-1} from the *B–H* plot.[33] For obtaining the limit of detection of H^+, it was calculated by determining the slope of the linearly fitting graph and standard deviation of the blank solution of probe **DSPH** fluorescence spectra. The limit of detection was determined to be 198 pM. Upon addition of TFA in increasing equivalents, a change in colour under UV lamp (365 nm) was observed from blue to yellow Fig. 5b.

3.8 pH and time response

After the analysis of spectroscopic variations in **DSPH** on the absorption and emission spectrum showing quenching of the probe in THF solution with the addition of TFA, it was further taken to study the effect of pH on the probe solution. The pH solutions from 2 to 12 were prepared with a neutral buffer solution which was further carefully adjusted to different pH using hydrochloric acid and base triethylamine (Et_3N) on a pH meter instrument. The change in the pattern for FL intensity was spotted at varying pH levels (2–12) as depicted in Fig. 6a. At a pH range of 9–11, the fluorescence intensity is maximum indicating that this pH range is best suited for studies, as at the pH levels in the range of 6–8 the fluorescence intensity decreases, and the emission intensity further decreases while going towards the acidic pH in the range of 2–6 with an observable change in fluorescence colour under 365 nm ultraviolet lamp from blue in basic to yellow in acidic pH. The probe **DSPH** and **DSPH + TFA** complex were studied to understand the time for the coordination of H^+ from TFA with the probe, Fig. 6b. The emission intensity of probe alone was increased linearly with time, however as soon as probe is protonated no change in emission intensity even at prolonged time duration to 80 seconds. This indicates the quenching is very clear when the probe is protonated.

3.9 Paper strip application

To comprehend the real-time application of probe acting as a sensor for TFA analyte, paper kit analysis was performed (Fig. 7). A strip of Whatman filter paper was cut and further coated with a solution of probe followed by air drying. Later, TFA was injected into the paper on the strip using a micropipette, which was further brought under a UV lamp to observe the change in fluorescence from blue to cyan-green to pale yellow at the spot with max TFA concentration.[34,35] The probe shows no solid-state fluorescence. The paper strips were verified for their long-term stability by keeping them as such in environment and verifying the change in fluorescence intensity. There were no observable changes in the strips for probe alone for 36 hours and beyond and with TFA the strips were stable till 28 hours and beyond.

3.10 Theoretical investigations

Gaussian 16 software is used for the density functional theory (DFT) calculations on **DSPH** with TFA. The 6-31G (d,p) basis set and the B3LYP correlation function were used together. The

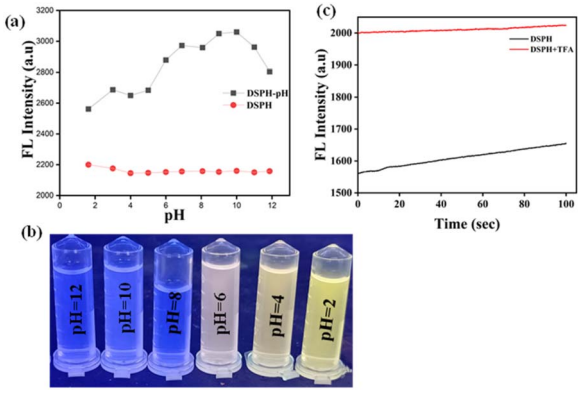

Fig. 6 (a) Emission intensity change based on varying pH (2–12) solutions, (b) bottle images representing the change in colour of fluorescence under UV lamp, (c) time scan studies for **DSPH** and **DSPH + TFA** complex.

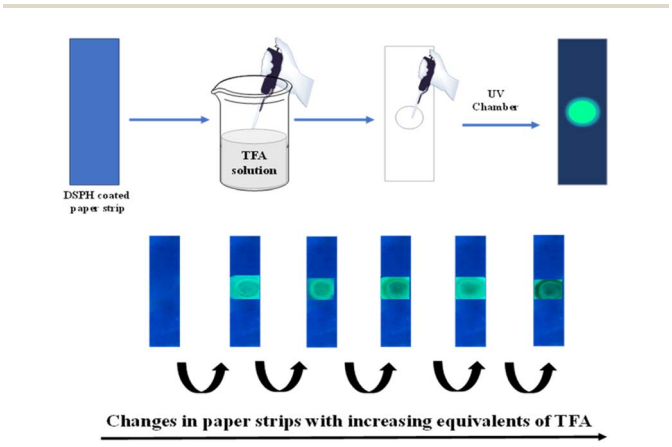

Fig. 7 Detection of TFA(H^+) using Whatman paper strips coated with probe **DSPH** solution.

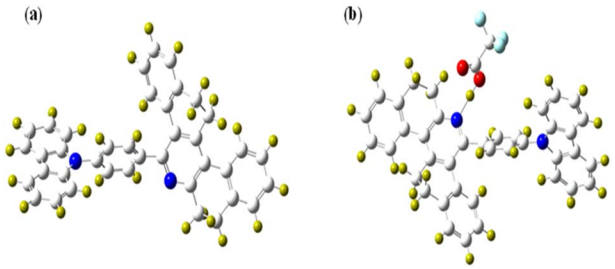

Fig. 8 Optimized geometry of (a) probe DSPH, (b) DSPH + TFA complex.

optimal structures of the executed chemical for complexes and probes[36] were obtained (Fig. 8). Before complexation, the energy gap between HOMO and LUMO values of 5.51 and 1.72 eV of **DSPH** was found to be 3.79 eV, and after complexation, we obtained a complex band gap of 3.52 eV for the values of 5.57 and 2.05 for HOMO and LUMO respectively (Fig. 9). There is a minor reduction. This suggests a stable sensor complex representing ligand-to-proton charge transfer for **DSPH** with TFA. The **DSPH** and **DSPH** with TFA are depicted in the figures, where the carbazole group is represented by the HOMO electron density across the electron spreading. The electron density is distributed throughout the molecule, apart from the phenanthridine group, when we approach LUMO. Also, the values for HOMO/LUMO of **DSPH** are in symmetry with the experimental values obtained from CV, which suggests substantial evidence for the reliability and accuracy of the computational approach. Moreover, the interaction energy between TFA and receptor were calculated using QTAIM (quantum theory of atoms in molecules – H-bond), depicting the interaction energy between N–H bond formed during complex formation, which turned out to be 80.168 kJ mol^{-1} providing information about the stability as well, suggesting a certainly strong complex formation and hence the stability of the complex (ESI Fig. S10†).

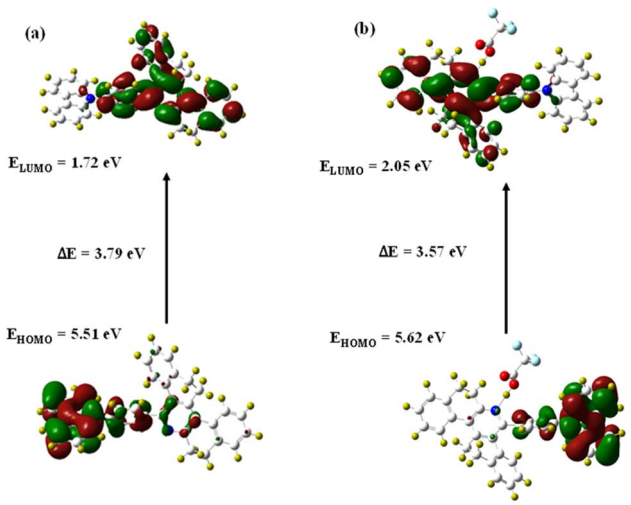

Fig. 9 Computed electronic distribution in the frontier molecular orbitals at B3LYP/6-31G (d,p) level: (a) for probe DSPH, (b) for DSPH + TFA complex.

4. Conclusion

The work effectively describes the synthesis of a novel carbazole-coupled phenanthridine probe displaying aggregation induced emission. The probe is also found to be thermally and electrochemically stable which is confirmed by its decomposition temperature value of 370 °C and the energy gap values determined *via* cyclic voltammetry between HOMO–LUMO, which were consistent with the theoretical investigations made by density functional theory approach. The probe displayed its use as a sensor for TFA *via* quenching mechanism and various photophysical parameters performed, proved its efficiency for the former. **DSPH** as a probe is a material of potential applications; one of them which this paper describes is it as a TFA sensor. Also, it holds potential to be used as a material in various optoelectronic devices.

Data availability

The data supporting this article have been included as part of the ESI.†

Conflicts of interest

The authors declare no conflict of interest.

Acknowledgements

The authors thank VIT for the facilities provided. VIT SIF is thanked for NMR and other sophisticated facilities. The authors also thank Dr Srinivasan, SSL-VIT for language editing.

References

1 J. K. Salunke, F. L. Wong, K. Feron, S. Manzhos, M. F. Lo, D. Shinde, A. Patil, C. S. Lee, V. A. L. Roy and P. Sonar, *J. Mater. Chem. C*, 2016, **4**, 1009–1018.
2 H. Shi, D. Xin, X. Gu, P. Zhang, H. Peng, S. Chen, G. Lin, Z. Zhao and B. Z. Tang, *J. Mater. Chem. C*, 2016, **4**, 1228–1237.
3 C. Poriel and J. Rault-Berthelot, *Adv. Funct. Mater.*, 2021, **31**, 2010547.
4 J. Luo, Z. Xie, J. W. Lam, L. Cheng, H. Chen, C. Qiu and B. Z. Tang, *Chem. Commun.*, 2001, **18**, 1740–1741.
5 A. Sharma, D. Saklani, K. R. J. Thomas, S. S. Swayamprabha and J.-H. Jou, *Org. Electron.*, 2020, **86**, 105864.
6 P. Cias, C. Slugovc and G. Gescheidt, *J. Phys. Chem. A*, 2011, **115**, 14519–14525.
7 P. Han, Z. Xu, C. Lin, D. Ma, A. Qin and B. Z. Tang, *J. Mater. Chem. C*, 2020, **8**, 7012–7018.
8 J. Guo, L. Pan, B. Song, J. Gu, J. Zeng, X. Xu, H. Wu, Z. Zhao, Z. Wang and A. Qin, *J. Mater. Chem. C*, 2019, **7**, 11160–11166.
9 C.-Y. Ho, G. Krucaite, R. Beresneviciute, D. Blazevicius, W.-H. Lin, J.-C. Lu, C.-Y. Lin, S. Grigalevicius and C.-H. Chang, *Org. Electron.*, 2022, **108**, 106571.
10 R. Isci, E. Tekin, K. Kaya, S. P. Mucur, S. F. Gorkem and T. Ozturk, *J. Mater. Chem. C*, 2020, **8**(23), 7908–7915.

11 G. Li, J. Zheng, K. Klimes, Z. Q. Zhu, J. Wu, H. Zhu and J. Li, *ACS Appl. Mater. Interfaces*, 2019, **11**(43), 40320–40331.
12 J. Jayabharathi, S. Thilagavathy and V. Thanikachalam, *Mater. Adv.*, 2021, **2**(15), 5160–5170.
13 X. Sun, L. Zhao, X. Han, H. Liu, Y. Gao, Y. Tao and P. Lu, *Molecules*, 2018, **23**(1), 190.
14 L. Shi, Z. Liu, G. Dong, L. Duan, Y. Qiu, J. Jia, W. Guo, D. Zhao, D. Cui and X. Tao, *Chem.–Eur. J.*, 2012, **18**, 8092–8099.
15 A. Sharma, R. Balasaravanan, K. R. J. Thomas, M. Ram, D. K. Dubey, R. A. K. Yadav and J.-H. Jou, *Dyes Pigm.*, 2021, **184**, 108830.
16 S. Seenan, S. Manickam, S. Sawminathan, D. Jothi and S. Kulathu Iyer, *J. Photochem. Photobiol., A*, 2022, **430**, 113952.
17 F. Monnier and M. Taillefer, *Angew. Chem., Int. Ed.*, 2009, **48**(38), 6954–6971.
18 G. Reddy, N. Duvva, S. Seetharaman, F. D'Souza and L. Giribabu, *Physics*, 2018, **20**(43), 27418–27428.
19 J. Zhang, F. Lu, S. Qi, Y. Zhao, K. Wang, B. Zhang and Y. Feng, *Dyes Pigm.*, 2016, **128**, 296–303.
20 K. I. Sathiyanarayanan, N. S. Karthikeyan, P. G. Aravindan, S. Shanthi, R. S. Rathore and C. W. Lee, *J. Heterocycl. Chem.*, 2009, **46**(6), 1142–1144.
21 S. Liu, Y. Li, R. T. K. Kwok, J. W. Y. Lam and B. Z. Tang, *Chem. Sci.*, 2021, **12**, 3427–3436.
22 L. Biesen, D. Woschko, C. Janiak and T. J. Müller, *Chem.–Eur. J.*, 2022, **28**(61), e202202579.
23 S. Ma, S. Du, G. Pan, S. Dai, B. Xu and W. Tian, *Aggregate*, 2021, **2**(4), e96.
24 W. Z. Yuan, P. Lu, S. Chen, J. W. Lam, Z. Wang, Y. Liu and B. Z. Tang, *Adv. Mater.*, 2010, **22**(19), 2159–2163.
25 Y. Yuan, S. Xu, C. J. Zhang and B. Liu, *Polym. Chem.*, 2016, **7**(21), 3530–3539.
26 X. Wang, Y. Yang, Y. Zhuang, P. Gao, F. Yang, H. Shen and D. Wu, *Biomacromolecules*, 2016, **17**(9), 2920–2929.
27 J. Jiao, J.-X. Kang, Y. Ma, Q. Zhao, H. Li, J. Zhang and X. Chen, *Front. Chem.*, 2019, **7**, 768.
28 H. Shi, S. Wang, L. Qin, C. Gui, X. Zhang, L. Fang, S. Chen and B. Z. Tang, *Dyes Pigm.*, 2018, **149**, 323–330.
29 G. Sathiyan and P. Sakthivel, *Dyes Pigm.*, 2017, **143**, 444–454.
30 X. Niu, H. Zhang, X. Wu, S. Zhu, H. Feng and W. Liu, *J. Mol. Struct.*, 2022, **1259**, 132754.
31 Y. Chen, B. Bai, Q. Chai, M. Zhang, J. Wei, H. Wang and M. Li, *Soft Matter*, 2019, **15**(33), 6690–6695.
32 M. Shellaiah, T. Simon, V. Srinivasadesikan, C.-M. Lin, K. W. Sun, F.-H. Ko, M.-C. Lin and H.-C. Lin, *J. Mater. Chem. C*, 2016, **4**, 2056–2071.
33 P. Thordarson, *Chem. Soc. Rev.*, 2011, **40**(3), 1305–1323.
34 H. Wang, L. Da, L. Yang, S. Chu, F. Yang, S. Yu and C. Jiang, *J. Hazard. Mater.*, 2020, **392**, 122506.
35 C.-X. Liu, J. Zhao, R.-R. Zhang, Z.-M. Zhang, J.-J. Xu, A.-L. Sun, J. Chen and X.-Z. Shi, *J. Hazard. Mater.*, 2020, **389**, 121884.
36 S. K. Lanke and N. Sekar, *Dyes Pigm.*, 2016, **124**, 82–92.